Check for updates

Relationships between structure, memory and flow in sheared disordered materials

K. L. Galloway [1], E. G. Teich [2], X. G. Ma[3,4], Ch. Kammer[1], I. R. Graham[5], N. C. Keim[6], C. Reina[1], D. J. Jerolmack[1,7], A. G. Yodh [5] and P. E. Arratia [1]✉

A fundamental challenge regarding disordered solids is predicting macroscopic yield—the point at which elastic behaviour changes to plastic behaviour—from the microscopic arrangements of constituent particles. Yield is accompanied by a sudden and large increase in energy dissipation due to the onset of plastic rearrangements. This suggests that one path to understanding bulk rheology is to map particle configurations to their mode of deformation. Here, we subject two-dimensional dense colloidal systems to oscillatory shear, measure the particle trajectories and bulk rheology, and quantify particle microstructure using excess entropy. Our results reveal a direct relation between excess entropy and energy dissipation that is insensitive to the nature of interactions amongst particles. We use this relation to build a physically informed model that connects rheology to microstructure. Our findings suggest a framework for tailoring the rheological response of disordered materials by tuning microstructural properties.

Disordered solids are ubiquitous. They are found, for example, in our foods as pastes and gels[1], and amidst our homes in the form of concrete[2] and mud[3,4]. Frustratingly, these materials can experience sudden mechanical failure, such as the collapse of soil during rapid mudslides. Indeed, when sufficiently stressed, all disordered materials exhibit a swift decrease in their ability to support load. In the vicinity of this yield transition, the solid material shifts from a state wherein energy is stored via internal elastic forces to a state in which energy is dissipated via irreversible plastic rearrangements[5,6]. Microscopic spatiotemporal features are associated with this yield transition and affect macroscopic material responses such as ductile versus brittle behaviour. In contrast to the case of crystalline materials, it remains a challenge to predict and control yield in disordered solids based on their constituents and interactions[7,8]. To build such microstructural models, we need to identify key microscopic metrics[9] relevant to plasticity in disordered materials. Recently, excess entropy has been explored for this purpose[10–12].

In equilibrium systems, the Rosenfeld scaling[13] has shown that inter-particle structure, measured by excess entropy, is connected to viscosity and particle mobility. Isomorph theory provides a framework for this connection[13,14]. Great strides have also been made in the use of entropy-based methods to describe the glass transition within a thermodynamic context. One such example is random first-order transition theory[15], which accounts for the system's entropy in excess of a crystalline state. In equilibrium, it is known that the largest contributions to the sample excess entropy are from local structures with low configurational entropy and thus decreased particle mobility[16]. Recently in far-from-equilibrium systems, excess entropy scaling has been shown to facilitate a relationship between microscopic structure and dynamics in simulations[11,12] and in experiments[10], but no relationship to nonlinear rheology is provided. Thus, excess entropy offers an untapped signature for plasticity and a potential tool for modelling the mechanical response of disordered solids.

The study of rheology and particle dynamics in disordered systems has a venerable history[17]. As a result of this research, theories have proliferated[9] in recent decades. Two of the most successful are mode coupling theory, wherein the interplay of dynamical modes causes the emergence of rearrangements[18], and shear transformation zone theory, which posits that local configurations determine where rearrangements occur[5,17,19]. More recently, structural signatures for rearrangement have been revealed by machine learning approaches[20], by study of low-frequency excitations[21,22] and via local yield stress[23,24] and near-neighbour cage dynamics[25]. Despite their usefulness, difficulties remain in applying these theories to experiments because of the need for fitting parameters[18,26] and the use of empirical relations[25] that are difficult to measure. Moreover, whilst these theories account for history dependence, an explicit phenomenological link between microstructure and history-dependent rheology has yet to be uncovered.

Generally, disordered materials contain memories, that is, microscopic signatures related to how the material has been processed[27–30]. Memory of a previous shearing direction, for example, can be encoded into a material's response. Once a material is sheared sufficiently in a given direction, continued shear requires more force than in the opposite direction because of a restoring force. In contrast, the Bauschinger effect is a memory at zero strain of previous plastic deformation. The yield stress is higher if sheared in the same direction as the original plastic deformation[5,24,31]. Both types of directional memory are related to the orientations of shear transformation zones[26] and have been described by shear transformation zone theory[5]. In jammed systems, recent experiments and simulations have studied directional memories at low strain amplitudes, both below and near the yield transition. Far above yield, memories are erased[32–34]. These observations, in turn, raise important new questions: How is microstructure related to directional memories? Is plastic flow synonymous with erasure?

[1]Department of Mechanical Engineering and Applied Mechanics, University of Pennsylvania, Philadelphia, PA, USA. [2]Department of Bioengineering, University of Pennsylvania, Philadelphia, PA, USA. [3]Center for Complex Flows and Soft Matter Research, Southern University of Science and Technology, Shenzhen, China. [4]Department of Physics, Southern University of Science and Technology, Shenzhen, China. [5]Department of Physics and Astronomy, University of Pennsylvania, Philadelphia, PA, USA. [6]Department of Physics, Pennsylvania State University, State College, PA, USA. [7]Department of Earth and Environmental Science, University of Pennsylvania, Philadelphia, PA, USA. ✉e-mail: parratia@upenn.edu
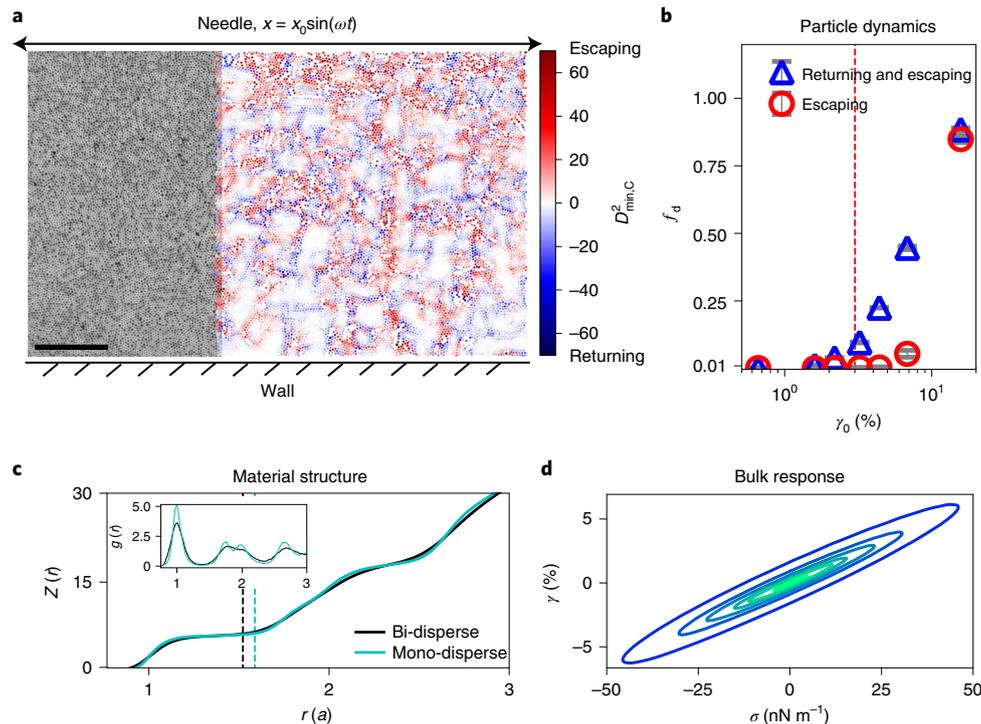
Fig. 1 | Overview of structure, dynamics and response. We characterize the disordered solid bulk response to cyclic stress from evolving configurations of individual constituent particles. **a**, Image of ~40,000 particles. Left: part of the raw image. Scale bar 200 μm. Right: detected particle positions. For illustration, colour indicates $D^2_{\min,C}$, which quantifies the degree to which a particle has followed a non-affine returning trajectory (blue) or a non-affine escaping trajectory (red). The particles in this image are experiencing yield ($\gamma_0 \approx 15.7\%$). **b**, Quantification of the fractions of particles escaping and returning averaged over all stress cycles versus total strain amplitude. Error bars show the s.d. over successive cycles of shear. Returning events rapidly increase near the yield point ($\gamma_0 \approx 3.0\%$). **c**, The number of particles $Z(r)$ within a radius r of a reference particle. The radius is expressed in units of a, the average distance between neighbouring particles. Vertical dashed lines indicate the limit of the first shell of neighbouring particles. Inset: the radial distribution function $g(r)$. **d**, The measured strain of the material versus the imposed stress throughout a cycle. Both stress and strain are averaged stroboscopically over 25 cycles. The different ellipses correspond to separate runs at different imposed stress amplitudes. Here, the area enclosed is a result of the lag between stress and strain, which in turn quantifies the energy dissipated from the material.

How do these phenomena manifest during yield, for example, in storage and loss moduli?

In this contribution, we utilize excess entropy to quantify material memory and construct a microstructural model for the response of and energy dissipation in disordered materials. Experiments and simulations show that three non-dimensional parameters govern the connections between microstructure and bulk rheology: packing density, a normalized (non-dimensional) form of the imposed stress and an excess entropy (microstructure-related) ratio that quantifies the material's ability to retain information about its initial state. Our results confirm that memory is stored elastically and lost plastically, and show how yield and the ductile/brittle response emerge from knowledge about particle configurations at the microscopic scale.

Results

The experiments investigate disordered solids. The solids are colloidal monolayers of (~40,000) athermal spherical particles adsorbed at an oil–water interface (Fig. 1a). The charged particle surfaces generate a dipole–dipole repulsion between particles. This repulsion is strong enough to jam the entire material, arresting particle motions. To probe the effects of disorder, we study both mono- and bi-disperse spherical particle systems with diameters of 5.6 μm and 4.1–5.6 μm, respectively. In the bi-disperse system, crystalline domains tend to be much smaller (see Sect. 1.1 of the Supplementary Materials). We impose many cycles of sinusoidal stress on these samples using a custom-made interfacial stress rheometer[33] that

permits measurement of the bulk response of the colloidal monolayer whilst simultaneously recording trajectories of individual particles (Methods). Cyclic stress is quasi-static insofar as the time scale for the completion of a rearrangement (~0.5 s) is much shorter than the shortest driving period (5 s) or largest inverse strain rate (20 s).

We investigate particle rearrangements by identifying non-affine deformations within each particle's neighbourhood[5,33]. The degree of non-affinity is quantified by the mean squared displacement after subtracting the best-fit affine transformation, $D^2_{\min}$ (see refs. [5,33] for more information). Within cyclically sheared disordered materials, two types of non-affine events occur (Fig. 1a): those wherein particles return to their original position at the end of a strain cycle but along different paths, and those wherein particles escape their nearest neighbours and do not return[35–38]. It is possible to concurrently measure the degree of returning and escaping non-affine behaviour for each particle[33]. For visualization, we estimate which type of non-affine event is dominant by defining $D^2_{\min,C} \equiv \pm\sqrt{(D^2_{\min,R})^2 + (D^2_{\min,E})^2}$, where the subscripts 'R' and 'E' refer to returning and escaping events, respectively. The sign for each particle is assigned according to which is greater. Negative corresponds to $D^2_{\min,R}$, whereas positive corresponds to $D^2_{\min,E}$. Both types of events dissipate energy[35–38]. Returning non-affine events are known to emerge near the yield point when elasticity begins to diminish and plasticity starts to increase[6,33]. Escaping events arise well beyond yield[33] (Fig. 1b). The fraction of particles undergoing non-affine events is f_d. By following the rearrangements, we develop
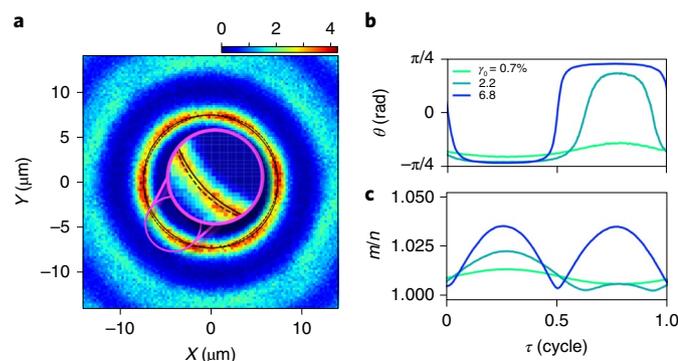
Fig. 2 | Memory within microstructure. Microstructural anisotropy reveals signatures of memory. Below yield, anisotropic orientation remains unchanged regardless of shear direction. Orientation quantifies stored memory. Above yield, anisotropic orientation reverses freely to match the direction of shear, indicating a loss of memory. **a**, Radial distribution function, $g(x, y, t)$, at a time corresponding to one/quarter of the way through a shearing cycle. We fit an ellipse to the first neighbour ring. This ellipse stretches and reorients over time, indicating changes in structural anisotropy of the sample. Two elliptic fits are shown at two times, $t = 1.25$ (solid line) and 1.75 cycles (dashed line). **b**, Orientation of the sample microstructure over time as a function of strain amplitude. With increasing strain amplitude, the microstructure reorients to match the stretching axis. It first reorients completely at the yield point (3.2%). **c**, Elongation quantified by the ratio of ellipse major and minor axis lengths (m/n) over time. Below yield, elongation oscillates directly with the strain; above yield, elongation oscillates with twice the frequency of strain perturbation. Data in **b** and **c** are averaged stroboscopically over 25 cycles.

understanding about trajectory dynamics within the microstructure and take steps towards our ultimate goal of relating microstructure to rheology.

To quantify structure, we characterize the inter-particle forces and particle configurations using the radial distribution function $g(r)$. Since the material is jammed, the motion of each particle is arrested by its neighbours[39–41]. This caging, and escape therefrom, provides another lens for the non-affine motions mentioned above. When enough particles pass each other via small changes in the structure of their surrounding cage, the material yields[5]. For quantitative analysis, we compute a microstructural measure of internal force, F^*, which is the sum of the magnitudes of inter-particle forces acting on the average particle. Specifically: $F^* = 2\pi\rho \int_0^{r_N} \left(-\frac{\partial u}{\partial r}\right) g(r) r \, dr$, where ρ is the number density of particles, r_N is an upper cutoff distance below which nearest-neighbour particles are found, u is the pair potential function between any two particles, $\frac{\partial u}{\partial r}$ is the force acting between any two particles and $g(r)$ is the sample radial distribution function as a function of separation r (Fig. 1c and Methods). To determine r_N, we use the coordination number as a function of radial distance, $Z(r)$ (Fig. 1c). $Z(r)$ is derived from $g(r)$ and has been studied[39] and recently used[25] to characterize particle interactions and their effect on bulk materials. In our systems, neighbour shells are well defined by broad peaks in $g(r)$ separated by troughs (Fig. 1c, inset). The extent of the nearest-neighbour shell is defined as the radius at which $Z(r)$ begins to increase rapidly for a second time (Fig. 1c).

We quantify disorder using excess entropy[13], the difference between the system's entropy and that of its ideal gas analogue (at identical pressure, temperature, etc.). The two-body approximation of excess entropy, s_2, is calculated from $g(r)$ using equation (4). We calculate s_2 at discrete time points to characterize its variation within each shear cycle (see below). Since our systems are jammed, we interpret the below-yield system s_2 as 'frozen-in' excess entropy[15,42].

We seek to relate these microstructural parameters to bulk rheological properties. Recall that as the yield transition is approached from below, the strain will begin to lag behind the oscillatory imposed stress by a phase angle, δ. If $\delta = 0$ rad, then the material is fully elastic. If $\delta = \pi/2$ rad, then the material is fully viscous. In between, the material exhibits both elasticity and plasticity. The phase angle lag quantifies the dissipation (Fig. 1d) and encodes the ratio of the loss (plasticity) and storage (elasticity) moduli, $G''/G' = \tan(\delta)$. We will show how G''/G' is related to the microstructural and dynamical quantities described above (s_2, F^*, f_d).

Next, we examine structural disorder and its variation as a function of applied shear. The angle-dependent radial distribution function, $g(x, y)$, quantifies microstructural order (Fig. 2a). Crucially, a nearest-neighbour ring is observable in disordered systems composed of interacting particles. In our experiments, this ring deforms throughout shear (Fig. 2a and Supplementary Video), in agreement with previous observations[25,43–45]. Throughout shear, the central ring is ellipsoidal. We can readily track the orientation and elongation of the ellipse throughout the shear cycle (Fig. 2b,c). Ellipse orientation and elongation provide a measure of the sample anisotropy. Far above yield, as the material is sheared in one direction and then the other, the microstructural anisotropy switches between two principal strain axes (oriented at $\pi/4$ rad and $-\pi/4$ rad, counter-clockwise from horizontal in Fig. 2a); in this situation, microstructural anisotropy is responsive to the direction of imposed shear (Fig. 2b). Below yield, however, the microstructural anisotropy remains in its original orientation; shearing is not sufficient to overcome initial 'frozen/in' material structure. This phenomenon is apparent from changes in ring elongation (Fig. 2c) during the shear cycle. Note that above yield the microstructure elongates twice every shear cycle, at a frequency of 2ω, but below yield, the microstructure elongates only once per cycle at ω.

Microstructural anisotropy reveals a memory of the last direction in which the material was sheared above yield (Fig. 2). To remove internal stresses, each of our experiments is pre-sheared well above yield ($\gamma_0 \sim 50\%$). Nevertheless, this protocol imprints an anisotropy into the sample set by the last shear direction. Previously it was shown that this type of material memory is imprinted into $g(x, y)$ (refs. [32,46]). Here, we find that this memory imprint is associated with the principal directions of shear (Fig. 2). Once a memory is stored, the memory is retained as long as the material is sheared elastically. Precisely when the material yields, all memory is lost and the microstructure switches freely between both orientations. Taken together, these results indicate that materials store and express memories in the elastic regime but lose them in the plastic regime. Furthermore, we recently showed that orientational memory is stored most strongly within crystalline domains wherein particle rearrangements are most intensely suppressed[34].

We now use excess entropy to characterize and relate observations about imprinted memory to the system microstructure. Above yield, we find that the structural response is independent of the direction of shear (Fig. 3a; $\gamma_0 = 6.8\%$). When the material is sheared in either direction, the excess entropy increases and decreases as the shear is reversed. Ostensibly, the material cannot sustain a memory above yield because it is continually forced out of meta-stable states within the energy landscape. Near yield, however, the direction of shear has an effect on the structural response (Fig. 3a; $\gamma_0 = 2.2\%$). Note that s_2 does not increase as the material is sheared over the second half of a sinusoidal shear cycle. Finally, below yield, the direction of shear is important. Shear in one direction produces an increase in excess entropy, whereas shear in the other direction produces a decrease (Fig. 3a; $\gamma_0 = 0.7\%$).

As seen in Fig. 3b, the s_2 signals are sinusoidal. The first harmonic (ω) decays whilst the second harmonic (2ω) grows with increasing strain amplitude. The first harmonic is dominant below yield, whereas the second is dominant above yield. Therefore, the
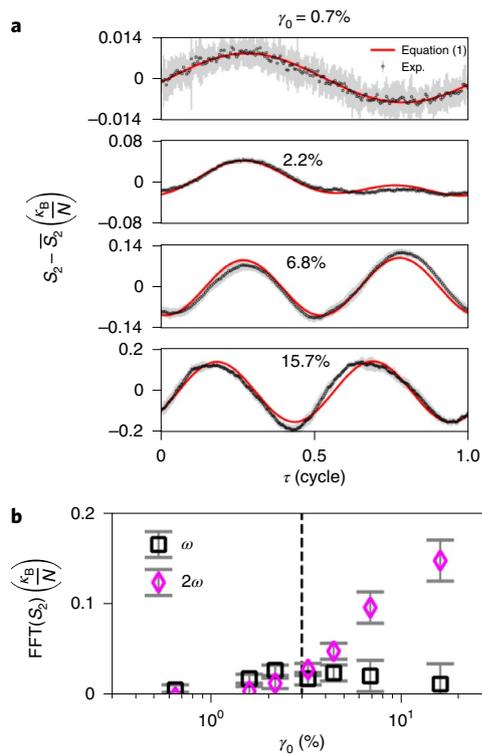
Fig. 3 | Entropy and material memories. Variation of entropy provides a means for predicting the system response to a given strain amplitude. **a**, Excess entropy, with the mean value subtracted, follows a sinusoidal response. Below yield, its oscillation frequency is the shear cycle frequency. At yield, the excess entropy signal has components at both the driving frequency and twice the driving frequency. The material is beginning to forget its initial state. Above yield, the entropy response oscillates almost exclusively at twice the shear cycle frequency. Black dots indicate experimental data. Red lines are fits to equation (1) with T as the only fitting parameter. The experimental data are averaged stroboscopically over 25 cycles. **b**, Amplitudes associated with the first and second harmonics are present within the s_2 signals. Note that the second and first harmonic amplitudes cross each other at the yield point, $\gamma_0 = 3\%$, indicated by the vertical dashed line. Error bars show the s.d. over all cycles.

amplitude of the first harmonic of s_2 provides quantification of a stored memory, and the amplitude of the second harmonic characterizes the degree to which memory of the initial state is lost. Note that these first and second harmonic amplitudes cross each other near the yield point.

To construct a relationship between excess entropy and bulk rheology, we next investigate the connection of s_2 to the other dynamical metrics. For this comparison, we compute the ratio of the second to first harmonic amplitude, which we denote as H_{s_2}. We can relate H_{s_2} to several quantities in our system (Fig. 4). For example, H_{s_2} scales with the product of F_0/F^* and f_d (Fig. 4a), where F_0 is the amplitude of the prescribed shear force. This relationship between dimensionless parameters suggests that, when the imposed force on the system grows larger than F^*, the microstructure begins to permanently change, losing stored memory. Rapid variation of f_d also signifies the transition. These findings build on recent work that links excess entropy and non-affine particle dynamics[10,11]. Note that the scaling in the present case is quadratic because f_d varies nearly linearly with the imposed force, F_0 (Supplemental Information and Fig. 3). Finally, we find that the product of $H_{s_2}^2$ and F^*/F_0 scales linearly with G''/G' (Fig. 4c). The scaling factor for this linear relationship is $2\phi/\pi^2$, where $\phi = \pi N a^2/A$ quantifies the particle spatial

density, a is the average nearest-neighbour distance derived from the first peak of $g(r)$ (Fig. 1c, inset) and A is the total area of the observed sample or simulation.

The yield phenomenology shown in Fig. 4c depends on four dimensionless parameters: F_0/F^*, H_{s_2}, G''/G' and the packing density ϕ. The ratio F_0/F^* characterizes the shear stress exerted on the material relative to the internal stress that the material contains. When $F_0/F^* \geq 1$, plasticity is non-negligible. The microstructural quantity H_{s_2} provides a metric for whether a material's response is dominated by memory as it experiences oscillatory strain. This microstructural property can be interpreted as the degree of plastic response. Finally, a familiar ratio quantifies the bulk rheological response of the material: (G''/G'). All experimental (and simulation) data are collapsed using these dimensionless parameters, and a direct relationship between rheology, dynamics and microstructure is experimentally established in the disordered solid.

Numerical simulations complement the experiments. The simulations enable us to vary features of the disordered system that are difficult to control experimentally. In particular, we can test ideas regarding variation of inter-particle potential. Moreover, unlike the experimental system, which involves a fluid–fluid interface that gives rise to viscous drag on the particles, the simulations offer the possibility to study the validity of our new concepts in disordered materials without viscous drag. Thus, we conducted shear simulations without viscous drag and with two different inter-particle interaction potentials: Lennard–Jones, a model for atomic glass, and Hertzian, a model for granular systems (Methods).

The simulations and experiments exhibit remarkably similar behaviours. Across both the experiments and simulations, a direct and common functional relationship between excess entropy and rheology is revealed (Fig. 4c). This relationship does not depend on the details of particle interactions nor the amount of disorder. Further, since simulations do not involve a background fluid, the importance of hydrodynamic effects is ruled out. The findings above measure how strongly a material can retain a memory when it is sheared. We can probe the limits of our findings by progressively making it harder for the simulations to form memories. One way to explore this issue is to introduce varying amounts of Brownian motion into the Lennard–Jones simulations. At low temperatures, particles are fully arrested by interactions with their neighbours. All mobility is due to shear, and memory is formed reliably. However, if temperature is so high that the particles rearrange due to Brownian motion, in addition to shear stress, then memory is not formed reliably. Thus, high temperatures that increase thermal mobility result in larger error bars in Fig. 4c. Similarly, in our Hertzian simulation, if the packing fractions are low enough that particles are not constrained by their neighbours, then memory is not formed reliably and quantitative relationships are observed to become noisier. The wide applicability of these ideas suggests the existence of a deeper theoretical formulation. Thus, in the remainder of this paper, we outline how our results may be derived phenomenologically (for the full derivation see Sect. 1.4 of the Supplementary Materials).

Inspired by the equilibrium successes of random first-order transition and related thermodynamic theories[15,42,47], we perform a simple energy balance to elucidate the relationship between s_2 and the material properties (G', G''). We start with the harmonic behaviour in s_2. In this situation, internal energy change is balanced via reversible heat transfer, $T\Delta S_2$, work, $F^*x/2$ and dissipation f_dFx (note that the change in internal energy is zero):

$$T\Delta S_2(t) = F^*x(t)/2 + f_dF(t)x(t). \tag{1}$$

Here, $x(t)$ is the displacement of the system boundary with respect to the equilibrium position $x(0) = 0$, $F(t)$ is the imposed shear force and T is a uniform scaling parameter (generally different from the
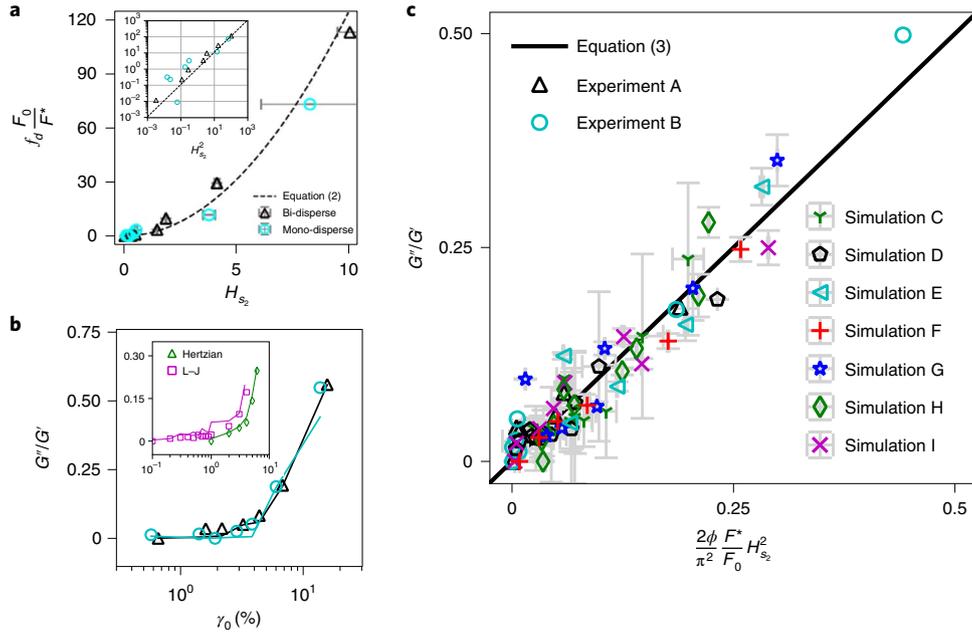
Fig. 4 | Comparisons of imposed force, microstructural excess entropy and bulk rheology. a, The imposed force amplitude, F_0, normalized by the elastic force capacity, F^*, versus the excess entropy harmonic ratio, H_{s_2} (in both mono-disperse and bi-disperse experiments). A fit of the data suggests a parabolic relationship ($P = 3.14 \times 10^{-13}$, and $r^2 = 0.989$), corroborating equation (2). Inset: log–log plot. **b**, The increase in the ratio of loss to storage moduli (G''/G') versus strain amplitude in both the mono-disperse and bi-disperse experiments (same legend for mono-disperse and bi-disperse experiments as in **a**). Yield is signalled by the rapid increase in parameter values at strain amplitude of about 0.03. Inset: data from simulations employing Hertzian and Lennard–Jones (L–J) interaction potentials. In both cases, markers are measured values and lines are predictions from equation (3). **c**, Left- and right-hand sides of equation (3). Notably, all parameters are measured. The solid diagonal line (slope 1.0) represents equation (3). The slope of the best fit to the data is 0.981 ($P = 4.43 \times 10^{-26}$ and $r^2 = 0.944$). All error bars are s.e.m.

thermal temperature) that converts differences in entropy to differences in energy within the representative cage[12,48–50]. This definition of T is in contrast to those from the Edwards ensemble[48], in which the equivalent parameter is the ratio of change of entropy to changes of volume or stress. Note that equation (1) quantifies the system-wide response via the average response of all cages (that is, a particle and its nearest neighbours) to the applied shear deformation. This equation would not apply in a system dominated by thermal motion because we do not account for changes in entropy due to thermal fluctuations. The term $F^*x/2$ is the work done by the surroundings on the cage (on average). This term is connected to the potential energy between particles. With a single fitting parameter, T, the changes in harmonic behaviour in excess entropy are reproduced from below to above yield (Fig. 3a).

The harmonic transition, associated with the excess entropy found in experiments and simulations, is captured by the first and second terms on the right-hand side of equation (1). $H_{s_2}^2$ is the ratio of those two terms:

$$H_{s_2}^2 = f_d \frac{F_0}{F^*}. \tag{2}$$

This relation describes the harmonics data remarkably well (Fig. 4a). We next build on equation (2) by incorporating a finding of shear transformation zone theory, namely that elastic energy builds up in the microstructure until it is plastically released via non-affine rearrangement events[5]. Quantitatively, this concept is represented as $G'' \propto Nf_dG'$, where N is the number of total particles observed. When substituted into equation (2), we obtain

$$\frac{G''}{G'} = \frac{2\phi}{\pi^2} \frac{F^*}{F_0} H_{s_2}^2. \tag{3}$$

Note that each parameter in this expression is measured and is generally accessible in many systems. Across strain amplitudes, remarkable agreement is found between G''/G' measured in experiments and simulations, and the predictions by equation (3) (Fig. 4b,c).

Conclusion

Our results demonstrate that the yield transition of jammed systems has a configurational origin rooted in the persistence of material memory. We investigated the responses of several jammed systems undergoing cyclic shear deformation, incorporating aspects of shear transformation zone theory, excess entropy and harmonic analysis into a single framework. The analysis reveals two new dimensionless parameters and three relations, derived phenomenologically, which connect particle configurations to bulk rheology. Importantly, the microstructural information needed, that is, the radial distribution function, is available in myriad scattering/microscopy experiments spanning length scales and particle types. Thus, this analysis is accessible to experimentalists. In the future, it should be interesting to search for similar relations for other loading conditions, such as compression or steady shear, and to explore a wider array of particulate systems in which the particles are not simple spheres. More specifically, it may also be possible to relate local excess entropy to separate plastic events by exploring a version of equation (1) and $F^*x/2$ that are applicable to individual cages on a case-by-case basis. Finally, it may be possible to generalize the work presented here to higher strain amplitudes by considering how energy is dissipated once f_d reaches unity.

We have developed a framework to understand bulk properties of jammed materials under shear based on microstructural information. The findings hold potential to predict behaviour of a broad range of dynamically arrested disordered materials including foams, gels, packings of nano- and micro-scale particles and atomic/

molecular glassy matter. Our findings may also shed light on some deeper questions, in particular, the nature of entropy and the potential to use entropy ideas in far-from-equilibrium media. Whilst entropy formulations for non-thermal systems have found utility in modelling disparate phenomena, its physical interpretation often remains mysterious. Disordered particulate packings appear to be particularly useful for clarifying this phenomenology since their material structure can be interrogated with relatively simple methods.

Online content

References

1. Nagel, S. R. Experimental soft-matter science. *Rev. Mod. Phys.* **89**, 025002 (2017).
2. Ioannidou, K. et al. Mesoscale texture of cement hydrates. *Proc. Natl Acad. Sci. U. S. A.* **113**, 2029–2034 (2016).
3. Jerolmack, D. J. & Daniels, K. E. Viewing Earth's surface as a soft-matter landscape. *Nat. Rev. Phys.* **1**, 716–730 (2019).
4. Nie, S., Jiang, Q., Cui, L. & Zhang, C. Investigation on solid–liquid transition of soft mud under steady and oscillatory shear loads. *Sediment. Geol.* **397**, 105570 (2020).
5. Falk, M. L. & Langer, J. S. Dynamics of viscoplastic deformation in amorphous solids. *Phys. Rev. E* **57**, 7192–7205 (1998).
6. Buttinoni, I. et al. Colloidal polycrystalline monolayers under oscillatory shear. *Phys. Rev. E* **95**, 012610 (2017).
7. Guazzelli, l & Pouliquen, O. Rheology of dense granular suspensions. *J. Fluid Mech.* **852**, P1 (2018).
8. Cipelletti, L., Martens, K. & Ramos, L. Microscopic precursors of failure in soft matter. *Soft Matter* **16**, 82–93 (2020).
9. Richard, D. et al. Predicting plasticity in disordered solids from structural indicators. *Phys. Rev. Mater.* **4**, 113609 (2020).
10. Galloway, K. L. et al. Scaling of relaxation and excess entropy in plastically deformed amorphous solids. *Proc. Natl Acad. Sci. U. S. A.* **117**, 11887–11893 (2020).
11. Ingebrigtsen, T. S. & Tanaka, H. Structural predictor for nonlinear sheared dynamics in simple glass-forming liquids. *Proc. Natl Acad. Sci. U. S. A.* **115**, 87–92 (2018).
12. Bonnecaze, R. T., Khabaz, F., Mohan, L. & Cloitre, M. Excess entropy scaling for soft particle glasses. *J. Rheol.* **64**, 423–431 (2020).
13. Dyre, J. C. Perspective: excess-entropy scaling. *J. Chem. Phys.* **149**, 210901 (2018).
14. Separdar, L., Bailey, N. P., Schrøder, T. B., Davatolhagh, S. & Dyre, J. C. Isomorph invariance of couette shear flows simulated by the sllod equations of motion. *J. Chem. Phys.* **138**, 154505 (2013).
15. Xia, X. & Wolynes, P. G. Fragilities of liquids predicted from the random first order transition theory of glasses. *Proc. Natl Acad. Sci. U. S. A.* **97**, 2990–2994 (2000).
16. Hallett, J. E., Turci, F. & Royall, C. P. Local structure in deeply supercooled liquids exhibits growing lengthscales and dynamical correlations. *Nat. Commun.* **9**, 1–10 (2018).
17. Argon, A. Plastic deformation in metallic glasses. *Acta Metal.* **27**, 47 – 58 (1979).
18. Siebenbürger, M., Fuchs, M., Winter, H. & Ballauff, M. Viscoelasticity and shear flow of concentrated, noncrystallizing colloidal suspensions: comparison with mode-coupling theory. *J. Rheol.* **53**, 707–726 (2009).
19. Slotterback, S. et al. Onset of irreversibility in cyclic shear of granular packings. *Phys. Rev. E* **85**, 021309 (2012).
20. Cubuk, E. D. et al. Structure-property relationships from universal signatures of plasticity in disordered solids. *Science* **358**, 1033–1037 (2017).
21. Chen, K. et al. Low-frequency vibrations of soft colloidal glasses. *Phys. Rev. Lett.* **105**, 025501 (2010).
22. Xu, N., Wyart, M., Liu, A. J. & Nagel, S. R. Excess vibrational modes and the boson peak in model glasses. *Phys. Rev. Lett.* **98**, 175502 (2007).
23. Patinet, S., Vandembroucq, D. & Falk, M. L. Connecting local yield stresses with plastic activity in amorphous solids. *Phys. Rev. Lett.* **117**, 045501 (2016).
24. Patinet, S., Barbot, A., Lerbinger, M., Vandembroucq, D. & Lemaître, A. Origin of the Bauschinger effect in amorphous solids. *Phys. Rev. Lett.* **124**, 205503 (2020).
25. Maestro, A. & Zaccone, A. Nonaffine deformation and tunable yielding of colloidal assemblies at the air–water interface. *Nanoscale* **9**, 18343–18351 (2017).
26. Bouchbinder, E. & Langer, J. S. Shear-transformation-zone theory of linear glassy dynamics. *Phys. Rev. E* **83**, 061503 (2011).
27. Keim, N. C. & Nagel, S. R. Generic transient memory formation in disordered systems with noise. *Phys. Rev. Lett.* **107**, 010603 (2011).
28. Mukherji, S., Kandula, N., Sood, A. & Ganapathy, R. Strength of mechanical memories is maximal at the yield point of a soft glass. *Phys. Rev. Lett.* https://doi.org/10.1103/PhysRevLett.122.158001 (2019).
29. Pashine, N., Hexner, D., Liu, A. J. & Nagel, S. R. Directed aging, memory, and nature's greed. *Sci. Adv.* https://advances.sciencemag.org/content/5/12/eaax4215.full.pdf (2019).
30. Keim, N. C., Hass, J., Kroger, B. & Wieker, D. Global memory from local hysteresis in an amorphous solid. *Phys. Rev. Res.* **2**, 012004 (2020).
31. Gadala-Maria, F. & Acrivos, A. Shear-induced structure in a concentrated suspension of solid spheres. *J. Rheol.* **24**, 799–814 (1980).
32. Keim, N. C., Paulsen, J. D. & Nagel, S. R. Multiple transient memories in sheared suspensions: robustness, structure, and routes to plasticity. *Phys. Rev. E* **88**, 032306 (2013).
33. Keim, N. C. & Arratia, P. E. Yielding and microstructure in a 2d jammed material under shear deformation. *Soft Matter* **9**, 6222–6225 (2013).
34. Teich, E. G., Galloway, K. L., Arratia, P. E. & Bassett, D. S. Crystalline shielding mitigates structural rearrangement and localizes memory in jammed systems under oscillatory shear. *Sci. Adv.* https://advances.sciencemag.org/content/7/20/eabe3392.full.pdf (2021).
35. Keim, N. C. & Arratia, P. E. Mechanical and microscopic properties of the reversible plastic regime in a 2D jammed material. *Phys. Rev. Lett.* **112**, 028302 (2014).
36. Lundberg, M., Krishan, K., Xu, N., O'Hern, C. S. & Dennin, M. Reversible plastic events in amorphous materials. *Phys. Rev. E* **77**, 041505 (2008).
37. Möbius, R. & Heussinger, C. (ir)reversibility in dense granular systems driven by oscillating forces. *Soft Matter* **10**, 4806–4812 (2014).
38. Regev, I., Lookman, T. & Reichhardt, C. Onset of irreversibility and chaos in amorphous solids under periodic shear. *Phys. Rev. E* **88**, 062401 (2013).
39. van Hecke, M. Jamming of soft particles: geometry, mechanics, scaling and isostaticity. *J. Phys. Condens.* **22**, 033101 (2009).
40. Behringer, R. & Chakraborty, B. The physics of jamming for granular materials: a review. *Rep. Prog. Phys.* **82**, 012601 (2018).
41. Liu, A. J. & Nagel, S. R. The jamming transition and the marginally jammed solid. *Annu. Rev. Condens. Matter Phys.* **1**, 347–369 (2010).
42. Martinez, L. & Angell, C. A. A thermodynamic connection to the fragility of glass-forming liquids. *Nature* **410**, 663–667 (2001).
43. Vermant, J. & Solomon, M. J. Flow-induced structure in colloidal suspensions. *J. Phys. Condens.* **17**, R187–R216 (2005).
44. Cheng, X., McCoy, J. H., Israelachvili, J. N. & Cohen, I. Imaging the microscopic structure of shear thinning and thickening colloidal suspensions. *Science* **333**, 1276–1279 (2011).
45. Seth, J. R., Mohan, L., Locatelli-Champagne, C., Cloitre, M. & Bonnecaze, R. T. A micromechanical model to predict the flow of soft particle glasses. *Nat. Mater.* **10**, 838–843 (2011).
46. Parsi, F. & Gadala-Maria, F. Fore-and-aft asymmetry in a concentrated suspension of solid spheres. *J. Rheol.* **31**, 725–732 (1987).
47. Dudowicz, J., Freed, K. F. & Douglas, J. F. *Generalized Entropy Theory of Polymer Glass Formation* (Wiley, 2007).
48. Bi, D., Henkes, S., Daniels, K. E. & Chakraborty, B. The statistical physics of athermal materials. *Annu. Rev. Condens. Matter Phys.* **6**, 63–83 (2015).
49. Ono, I. K. et al. Effective temperatures of a driven system near jamming. *Phys. Rev. Lett.* **89**, 095703 (2002).
50. Khabaz, F. & Bonnecaze, R. T. Thermodynamics of shear-induced phase transition of polydisperse soft particle glasses. *Phys. Fluids* **33**, 013315 (2021).

Methods

Experiments. Using a custom-built interfacial stress rheometer (Supplementary Fig. 1), we simultaneously measure storage and loss moduli and track particle positions in two-dimensional dense suspensions of athermal repulsive particles. The interfacial stress rheometer measures rheology by imposing force on a magnetic needle adsorbed at an interface between oil and water[51]. A stationary wall is opposite the needle, so that shear is imposed over a distance visible by a microscope. The displacement of the rod is measured precisely with the microscope. With displacement (strain) and imposed force (stress), the storage and loss moduli are calculated[52,53]. Additionally, the microscope is used to image the particles (~40,000, from wall to needle) adsorbed at the interface. The particles include charges on their surfaces, so they exert dipole–dipole repulsive forces on each other[54–56]. At the particle densities in these experiments, these forces result in particle jamming, which we define as full kinematic restraint on each particle by its neighbours. In all data reported here, the systems are in a sinusoidal steady state. In the experiments, steady state occurs after five shear cycles. Twenty-five steady-state cycles are used for calculations. For more information about these experiments and the calculations of $D_{\min}^2$, see refs. [33,35,57].

An accessible quantity in our experiments is the two-body approximation of excess entropy, the difference between the system's entropy and the entropy of an ideal gas in an equivalent state ($s_2 \sim s_{\text{sys.}} - s_{\text{I.G.}}$). Conveniently, this quantity is calculated from the radial distribution function, which is available in a wide range of experiments[58]. The previously derived[59] formula for excess entropy is

$$s_2 = -\pi\rho \int_0^\infty \{g(r)\ln[g(r)] - [g(r) - 1]\}\, r\, dr, \qquad (4)$$

where ρ is the particle number density. We implement equation (4) for each image in our experiments individually to collectively construct an entropy time signal, $s_2(t)$. For specifics of our excess entropy calculations, see ref. [10].

The network force F^* introduced herein is calculated based on inter-particle forces within the average neighbourhood of particles. To make this measurement, we estimate the average number of nearest neighbours around a particle as

$$Z(R_c) = 2\pi\rho \int_0^{R_c} g(r) r\, dr, \qquad (5)$$

where R_c values are shown on the horizontal axis in Fig. 1c. We estimate experimental inter-particle forces based on potentials measured in experiments and molecular dynamics simulations reported in ref. [56]. An account of our estimate is included in Sect. 1.3 of the Supplementary Information.

Simulations. The data points for samples C were obtained using LAMMPS[60]. At each strain amplitude, ten two-dimensional ensembles of 10,000 bi-disperse Lennard–Jones particles[23,61] were subjected to sinusoidal shear under periodic boundary conditions at constant confining volume. The period of shearing was 100× the Lennard–Jones time scale of the particles. Before shearing, the samples were dynamically equilibrated at 1% of the glass-transition temperature[23]. During strain-controlled shearing, LAMMPS' Nosé–Hoover thermostat was used to maintain the samples at approximately 1% of the glass-transition temperature. After 40 cycles of shearing, the shear stress was output for another 40 cycles for later use in the calculations of the dynamic moduli. We find that similar calculations at 9% of the glass-transition temperature begin to introduce noise into our final relation.

For simulation samples D and E, we use HOOMD-blue[62,63] to impose cyclic strain on ten particle configurations for each of six strain amplitudes (1%, 2%, 3%, 4%, 5% and 6%) at constant confining volume. Ensembles are composed of jammed states of 50:50 bi-disperse mixtures of 10,000 Hertzian particles. Ensembles are initialized from a randomly uniform probability distribution at a packing fraction below jamming, and subsequently quenched under fast inertial relaxation engine minimization[64] whilst increasing the packing fraction until the desired pressure is reached. We then run a triangle-wave shear protocol, imposing a small strain step of 10^{-4}% and minimizing under fast inertial relaxation engine after each step, until a total of 40 cycles have been completed. We calculate dynamic moduli based on the dominant frequencies of the resulting triangle waves.

Data availability

Source data are provided with this paper. All data that support the plots within this paper and other findings of this study are available from the corresponding author upon reasonable request. Source data are provided with this paper.

References

51. Shahin, G. *The Stress Deformation Interfacial Rheometer*. Ph.D. thesis, University of Pennsylvania (1986).
52. Brooks, C. F., Fuller, G. G., Frank, C. W. & Robertson, C. R. An interfacial stress rheometer to study rheological transitions in monolayers at the air/water interface. *Langmuir* **15**, 2450–2459 (1999).
53. Reynaert, S., Brooks, C. F., Moldenaers, P., Vermant, J. & Fuller, G. G. Analysis of the magnetic rod interfacial stress rheometer. *J. Rheol.* **52**, 261–285 (2008).
54. Aveyard, R., Clint, J. H., Nees, D. & Paunov, V. N. Compression and structure of monolayers of charged latex particles at air/water and octane/water interfaces. *Langmuir* **16**, 1969–1979 (2000).
55. Masschaele, K., Park, B. J., Furst, E. M., Fransaer, J. & Vermant, J. Finite ion-size effects dominate the interaction between charged colloidal particles at an oil–water interface. *Phys. Rev. Lett.* **105**, 048303 (2010).
56. Park, B. J., Vermant, J. & Furst, E. M. Heterogeneity of the electrostatic repulsion between colloids at the oil–water interface. *Soft Matter* **6**, 5327–5333 (2010).
57. Keim, N. C. & Arratia, P. E. Role of disorder in finite-amplitude shear of a 2D jammed material. *Soft Matter* **11**, 1539–1546 (2015).
58. Larson, R. *The Structure and Rheology of Complex Fluids* (Oxford Univ. Press, 2010).
59. Baranyai, A. & Evans, D. J. Direct entropy calculation from computer simulation of liquids. *Phys. Rev. A* **40**, 3817–3822 (1989).
60. Plimpton, S. *Fast Parallel Algorithms for Short-Range Molecular Dynamics* (Sandia National Labs, 1993).
61. Widom, M., Strandburg, K. J. & Swendsen, R. H. Quasicrystal equilibrium state. *Phys. Rev. Lett.* **58**, 706 (1987).
62. Glaser, J. et al. Strong scaling of general-purpose molecular dynamics simulations on gpus. *Comput. Phys. Commun.* **192**, 97–107 (2015).
63. Anderson, J. A., C. D., L. & Travesset, A. General purpose molecular dynamics simulations fully implemented on graphics processing units. *J. Comput. Phys.* **227**, 5342–5359 (2008).
64. Bitzek, E., Koskinen, P., Gähler, F., Moseler, M. & Gumbsch, P. Structural relaxation made simple. *Phys. Rev. Lett.* **97**, 170201 (2006).

Author contributions

D.J.J., A.G.Y. and P.E.A. designed the research. K.L.G. and N.C.K. conducted the experiments. Ch.K. and I.R.G. ran the simulations. The analysis and model were developed by K.L.G., C.R., X.G.M., A.G.Y. and P.E.A. All authors discussed the results and wrote the manuscript.

Competing interests

The authors declare no competing interests.

Additional information

Supplementary information The online version contains supplementary material available at https://doi.org/10.1038/s41567-022-01536-9.

Correspondence and requests for materials should be addressed to P. E. Arratia.

Peer review information *Nature Physics* thanks Francesco Turci and the other, anonymous, reviewer(s) for their contribution to the peer review of this work.

Reprints and permissions information is available at www.nature.com/reprints.